EPJ Web of Conferences **295**, 02004 (2024) https://doi.org/10.1051/epjconf/202429502004
CHEP 2023

ATLAS Liquid Argon Calorimeter Commissioning for LHC Run-3

Marin Furukawa[1,*] on behalf of the ATLAS Collaboration

[1]The University of Tokyo, 7-3-1 Hongo, Bunkyo Ward, Tokyo, Japan

Abstract. The Liquid Argon calorimeter of the ATLAS detector provides inputs to the first level of the ATLAS trigger. After the successful period of data-taking during the second run of the LHC (Run-2) the ATLAS detector entered into a long period of shutdown. In 2022 the LHC has started a new data taking period Run-3. During the Run-3 period (2022 - 2025), it expects to have higher luminosity than Run-2 with pile-up of up to 80 interactions per bunch crossing.

To cope with these harsh conditions, a new trigger readout system has been installed during the long shutdown. The new system should improve the triggering performances for electromagnetic objects significantly. This will be achieved by increasing the granularity of the readout system available at trigger-level by up to a factor of ten. This new trigger system is currently undergoing commissioning in order to become the main LAr trigger readout in 2023.

This contribution will present the current status of the Liquide Argon Calorimeter system and the commissioning to be completed towards the full operation of the new trigger readout system for Run-3 of the LHC.

1 The ATLAS Liquid Argon Calorimeter

The Liquid Argon (LAr) Calorimeter is employed by ATLAS for all electromagnetic calorimetry in the pseudo-rapidity region $|\eta| < 3.2$*, and for hadronic and forward calorimetry in the region from $|\eta| = 1.5$ to $|\eta| = 4.9$. It is a sampling calorimeter used to measure the transverse momentum magnitude (energy) E_{T} of electrons, photons and hadronic jets, using lead, copper and tungsten as absorber materials, and liquid argon as the active material. The region of $\eta < 0$ is called "C-side", while the positive η region is called "A-side". It is comprised of four sub-detectors shown in Figure 1a: The Electromagnetic Barrel (EMB) and Electromagnetic End-caps (EMEC) are electromagnetic calorimeters, the Hadronic End-cap (HEC) is hadronic calorimeter, and the Forward Calorimeter (FCal) is comprised of both of electromagnetic and hadronic calorimeters. There are around 200,000 channels in total, which comprise up to four layers, as shown in Figure 1b. The E_{T} measured in every bunch crossing (BC) by the LAr calorimeter is sent to the first level (L1) of the ATLAS trigger.

*e-mail: marin.furukawa@cern.ch

*ATLAS uses polar coordinates (η, ϕ) in the transverse plane, ϕ being the azimuthal angle around the z axis. The pseudorapidity is defined in terms of the polar angle θ as $\eta = -ln\tan(\theta/2)$. Angular distance is measured in units of $\Delta R \equiv \sqrt{(\Delta\eta)^2 + (\Delta\phi)^2}$.

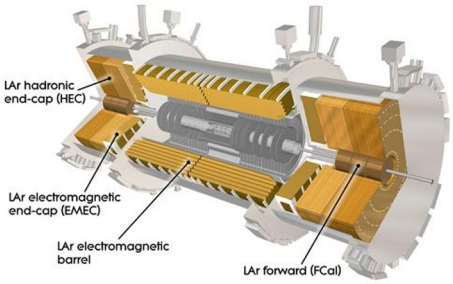

(a) Four sub-detectors of the LAr calorimeter. The full cryostat containing the EMB is 6.8 m long, with an outer radius of 2.5 m. Both ends including EMEC, HEC, and FCal are called End-caps. Each of these is 3.17 m long.

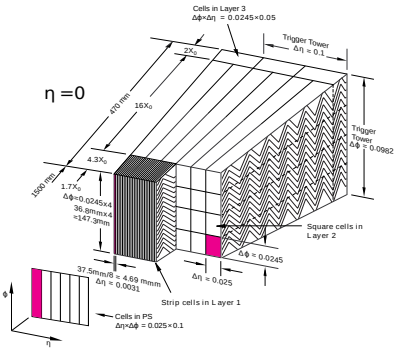

(b) The typical structure of layers for the EM calorimeters. The presampler (PS) layer is only present for $|\eta| < 1.8$. Layers 1, 2, and 3 are called "Front", "Middle", and "Back", respectively. The hadronic calorimeters have different structures.

Figure 1: The Liquid Argon Calorimeter [1]

2 Installation and commissioning timeline

The second run of the LHC (Run-2) finished in 2018, and the LHC was shut down from 2019 to the beginning of 2022. The trigger readout system of the LAr calorimeter was upgraded as "The phase-I upgrade" in preparation for "Run-3" (2022-2025) and the coming high-luminosity phase (HL-LHC). Hardware installation of the new trigger system was finished in 2021. The final commissioning is ongoing using Run-3 proton-proton collision data to make the new system as the main trigger readout in 2023.

3 Current status

A single beam which collides with a certain target and collimator, "splashes" the detector and injects particles into almost all channels. These "beam splash" events were performed before Run-3 pp collisions began. Figure 2 shows a beam splash event where the majority of LAr channels have energy deposits of o(10) GeV.

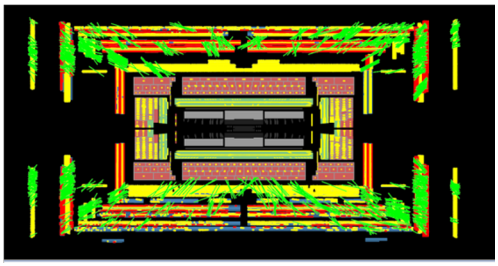

Figure 2: Event display for a single beam splash event taken on 28th March 2023 [2]. The beam entered from C-side in the direction of A-side (left to right). Green boxes show EMB, EMEC, and parts of FCal, and two red boxes next to the green boxes on the End-cap part show HEC and parts of FCal. Yellow blocks inside the boxes (EMB, EMEC, HEC, and FCal) show energy deposited in each box.

Figure 3 shows the energy deposited in a hypothetical tower grid with $\eta \times \phi = 0.025 \times 0.025$ during the beam splash event shown in Figure 2. Energy is reconstructed by elementary cells, which has been used in Run-2. It shows all of main readout works well and good coverage is achieved.

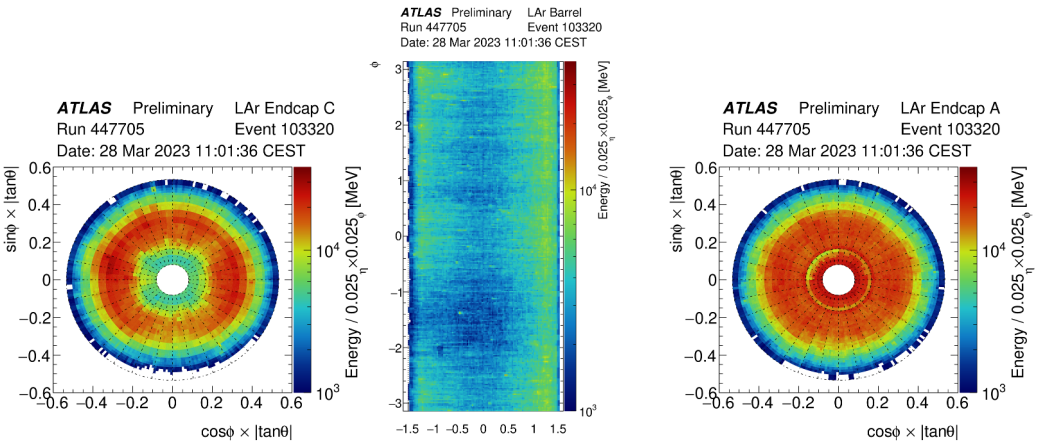

(a) Observed energy in End-cap C side.

(b) Observed energy in EMB.

(c) Observed energy in End-cap A side.

Figure 3: Coverage of energy deposited in elementary cells during a beam splash event [3]. The x and y axes corresponds to the location of each cell, and the z axis means accumulated energy deposited in each hypothetical tower grid of $\eta \times \phi = 0.025 \times 0.025$.

4 Phase-I Upgrade for trigger system

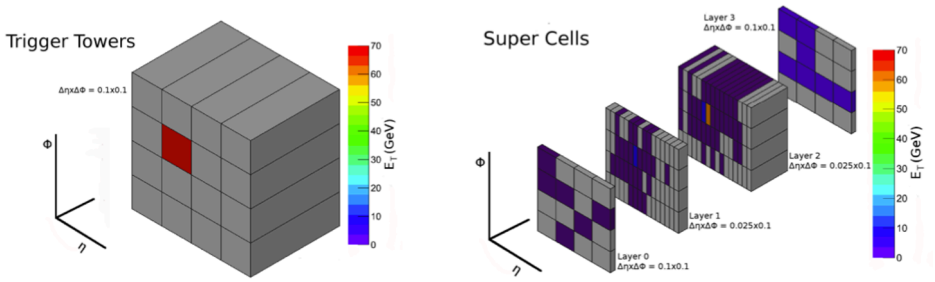

(a) "Trigger Tower", legacy readout units.

(b) "Super cell (SC)", upgraded readout units.

Figure 4: An electron with 70 GeV of transverse energy as seen by the legacy (4a) and upgraded digital (4b) trigger systems [1].

In Run-3 and the coming HL-LHC, the instantaneous luminosity has been increased. As a result, the background electromagnetic (EM) objects from such as inelastic scattering interactions (multi-jets) will be increased, too. However, the rate for EM objects in the L1 trigger can't be raised. The given rate of the single electron trigger is 20 kHz. If the E_{T} threshold

is increased to reduce the background EM objects, the trigger can miss the target signal. In order to avoid this, the digital trigger system was introduced to replace the analog trigger system used in Run-2. In trigger readout, the signals are processed by summing LAr cells to a certain readout unit. Not only the whole the system was replaced from analog to digital, but the readout unit was also changed to maximum ten times finer granularity "Super Cells (SC)" compared to the Run-2 "Trigger Towers" as shown in Figure 4. There are 34,048 SCs and they enable improved jet background suppression for EM triggers through the use of shower shape variables below:

$$R_\eta = \frac{E^{(2)}_{T,\Delta\eta\times\Delta\phi=0.075\times0.2}}{E^{(2)}_{T,\Delta\eta\times\Delta\phi=0.175\times0.2}} \tag{1}$$

$$f_3 = \frac{E^{(3)}_{T,\Delta\eta\times\Delta\phi=0.2\times0.2}}{E^{(1)}_{T,\Delta\eta\times\Delta\phi=0.075\times0.2} + E^{(2)}_{T,\Delta\eta\times\Delta\phi=0.075\times0.2} + E^{(3)}_{T,\Delta\eta\times\Delta\phi=0.2\times0.2}} \tag{2}$$

$$w_{\eta,2} = \sqrt{\frac{\sum (E^{(2)}_{\mathrm{T}} \times \eta^2)_{\Delta\eta\times\Delta\phi=0.075\times0.2}}{E^{(2)}_{T,\Delta\eta\times\Delta\phi=0.075\times0.2}} - \left(\frac{\sum (E^{(2)}_{\mathrm{T}} \times \eta)_{\Delta\eta\times\Delta\phi=0.075\times0.2}}{E^{(2)}_{T,\Delta\eta\times\Delta\phi=0.075\times0.2}}\right)^2} \tag{3}$$

The numbers in brackets indicate a layer and $\Delta\eta \times \Delta\phi$ indicates the range where the deposited E_{T} is summed up. R_η is defined as the E_{T} deposited in the 3×2 SCs divided by the E_{T} measured in 7×2 SCs, centered on the SC where the highest E_{T} of the middle layer, f_3 gives a fraction of E_{T} deposited in a back layer to that in front, middle, and back layer, and $w_{\eta,2}$ shows a spread of E_{T} deposited in 3×2 SCs in a middle layer. Using these variables, narrow EM objects ($R \sim 0.04$) can be separated from jet background ($R \sim 0.4$).

Figure 5 shows that the expected performance of the digital trigger readout shown in red squares is raised to efficiency 1 quickly after the threshold (22 GeV) while the analog trigger readout shown in black points reaches this efficiency at a much higher energy. This indicates that the digital trigger system achieves efficient object identification and maintains triggering efficiency without raising the threshold, with keeping trigger rate at 25 kHz.

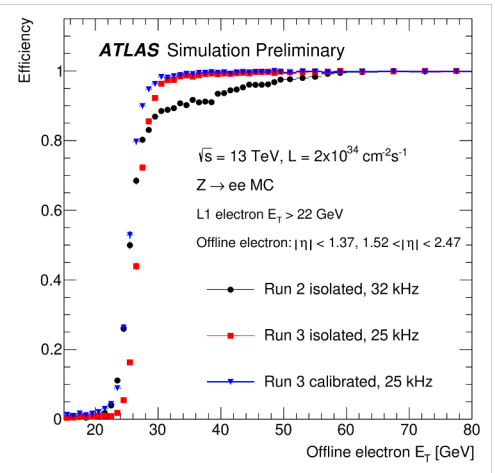

Figure 5: The expected Single-electron trigger efficiency computed from $Z \to ee$ Monte Carlo simulation [9].

5 The digital trigger system and the firmware

5.1 Trigger system

Figure 6 shows a schematic block diagram of the LAr calorimeter trigger system. "Tower Builder Board" and "Receiver" are parts of the legacy system which will be disabled. Protons collide at 40 MHz and interacting particles produce signals on channels of the LAr calorimeter. Pulses obtained from the particle hits are around 600 ns long. These are summed up to units of SCs by upgraded "New Layer Sum Boards (LSB)". Summed signals are sent through the Baseplane to the "LAr Trigger Digitizer Board (LTDB)". There are 114 Baseplanes and 124 LTDBs. Each signal is digitized at 40 MHz and sent through 80〜100 m of optical fiber to the "LAr Digital Processing System (LDPS)" with a total throughput of 40 Gbps per LDPS. The total data transmission rate is 25.2 Tbps. There are 31 Processors ATCA** blades, each with up to 4 AMCs*** called "LATOMEs". Then, the magnitude of transverse momentum is computed and sent through 10 m optical fibers to the L1 trigger system, with a total throughput of 40 Tbps.

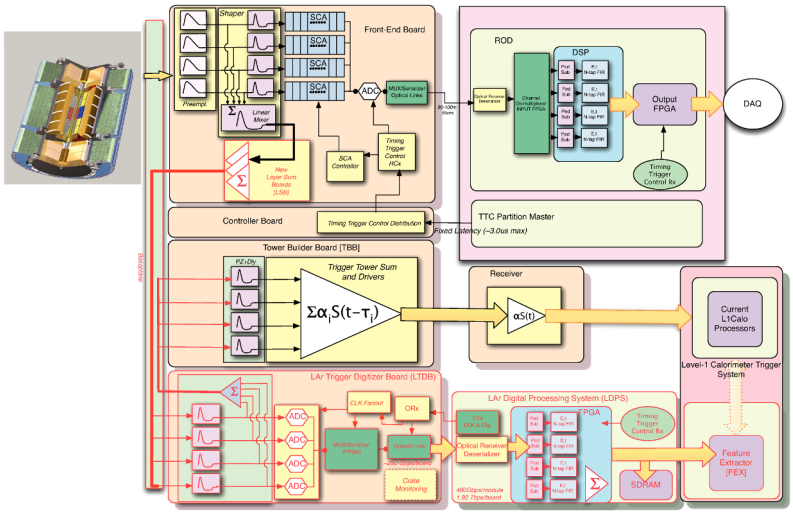

Figure 6: Schematic block diagram of the LAr trigger readout architecture [5]. The digital trigger system is indicated by the red outlines and arrows.

5.2 Firmware for digital processing

The LATOME uses 116 FPGAs**** (Intel Arria-10). The data is sent from the LTDB at 5.12 GHz per fiber. Data frames containing 8 SCs × 16 bits (including 12 bits for ADC) are sent to the first module of LATOME at 320 MHz. Data is recorded following the detector geometry for each BC and the clock frequency is reduced to 240 MHz in the second module for easier handling in the main module "User Code". This main module has three functionalities. The first functionality is to reconstruct E_{T} and injected timing τ. E_{T} and τ are reconstructed by "Optimal Filtering", a kind of Finite Impulse Response (FIR) computation shown in Eq. (4) in real-time at fixed latency of 125 ns.

**Advanced Telecommunications Computing Architecture
***Advanced Mezzanine Cards
****Field-Programmable Gate Array

$$E_{\mathrm{T}} = \sum_{i=0}^{3} \tilde{A}_{\mathrm{i}}(S_{\mathrm{i}} - p - b), \quad E_{\mathrm{T}}\tau = \sum_{i=0}^{3} \tilde{B}_{\mathrm{i}}(S_{\mathrm{i}} - p - b) \tag{4}$$

S_{i} is a ADC value of each data point, p is a pedestal, b is baseline level depending on the bunch structure, and $\tilde{A}_{\mathrm{i}}$ and $\tilde{B}_{\mathrm{i}}$ are "Optimal Filtering Coefficient (OFC)" computed for each SC. The second functionality is τ selection for the bunch crossing assignment, details of which are given in section 6. This provides identification of the BC from which the particle originates. It's necessary for the trigger. The third one is the detection of saturation (see Ref. [6]).

Following these steps, the data is formed in the final module to be sent to the L1 trigger. The L1 trigger receives the data at 11.2 Gbps per fiber via optical fibers. There are 40 fibers in total for each input and output per LATOME, approximately 8,200 fibers for the whole system. FPGA resource occupancy is very large: 92 % of logic units and 95 % of memory, while we have managed to avoid any timing violations.

6 Timing alignment for BC identification

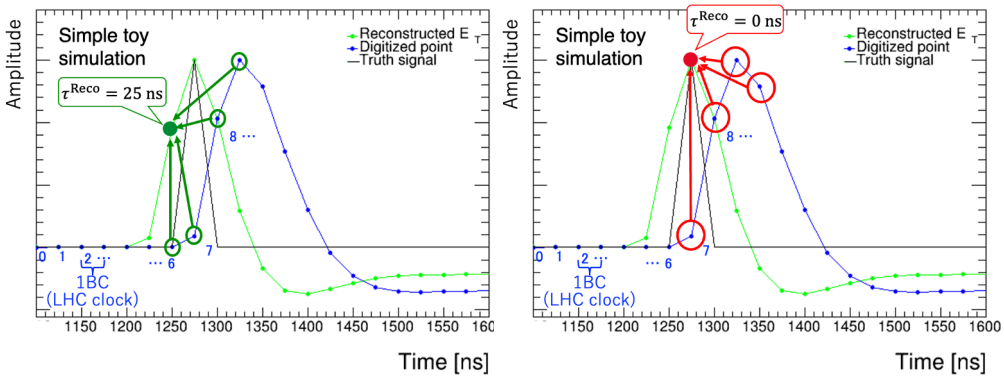

Figure 7: A simple toy simulation of a pulse. An injected signal is shown in black, digitized data points are shown in blue, E_{T} and τ reconstructed from blue points using optimal filtering are shown in green. The blue numbers represent BCIDs.

Pulses obtained from incident particles last around 600 ns; longer than the LHC collision frequency. The BCs from which these came from must be identified. Figure 7 describes the optimal filtering with a simple toy simulation using a LAr calibration pulse. Each BC is given an identification number from 0 to 3563, called the "Bunch Crossing Identifier (BCID)". The pulse is digitized at the same frequency as the LHC clock, and one BCID is associated with each of those points. At every BC, the τ and E_{T} are computed, and if the τ is 0 ns, the computed E_{T} is sent to the later stage, while the other entries are set to 0. To be specific, four points starting from BCID = 6, indicated by green circles in the left-hand plot of Figure 7, reconstruct a green point, and its reconstructed τ is 25 ns. The next four points starting from BCID = 7, indicated by red circles in the right-hand plot of Figure 7, reconstruct a red point, and its reconstructed τ is 0 ns. This means that this signal is generated in the BC where the BCID is 7, and the E_{T} for other points are set 0. Matching the BCID of the LHC with the BCID assigned to each data point is very important. The BCID assigned to each data point by the timing alignment is calibrated using collision data per fiber taking latency into account. All 4,458 fibers were scanned and calibrated in 2022.

7 Run-3 collision data after the timing alignment

Figure 8 shows comparisons of the E_{T} between the main readout and digital trigger readout using the stable beam pp collision data taken after the timing alignment described in Section 6. Figure 8a shows the 1D distribution of relative E_{T} difference between the readout paths, while Figure 8b shows a direct 2D E_{T} comparison between two. These two show good alignment. Especially, the EM Barrel has a good resolution. The numbers of 'good' and masked SCs are summarized in Section 8. The masked SCs and SCs affected by firmware configuration errors are omitted from the E_{T} comparisons shown in Figures 8. These results mean the digital trigger performs well as expected in case of no firmware or hardware errors. Since May 2023, the digital trigger system has taken over from the analog system to provide EM triggers. The trigger turn-on curves for the digital trigger are shaper, resulting from a higher efficiency and lower L1 rates at the same E_{T} threshold.

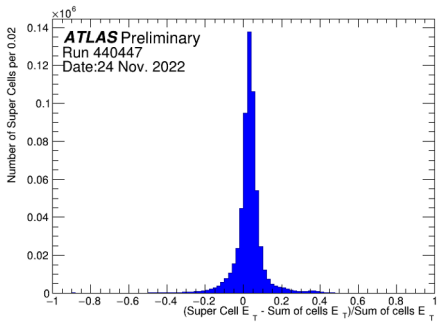

(a) Injected timing distribution.

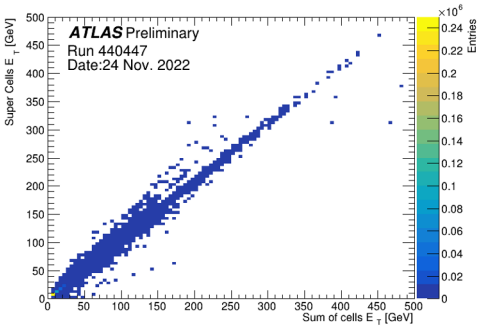

(b) E_{T} comparison. Scattered points above $y = x$ line come from the hadronic section.

Figure 8: Collision data taken after the timing alignment [7]. The Sum of cells E_{T} is the offline summed E_{T} reconstructed by the SC's constituent elementary cells. Super cells E_{T} is calculated in real time on the LATOME. Only hits which have an energy larger than 5 GeV and pass timing criteria, defined as -8 ns $< \tau <$ 14 nsfor10 GeV $< E_{\mathrm{T}}$ or -8 ns $< \tau <$ 8 nsfor0 GeV $< E_{\mathrm{T}} \leq 10$ GeV, are included.

8 Super cells status

There are 34,048 SCs, of which 33,494 have no issues and output the expected E_{T} and τ as of November 2022. 200 SCs are affected by a broken calibration board since April 2022, while 354 SCs have other issues related to their associated LTDBs or to the extraction of the OFCs. These 554 SCs are masked. The broken calibration board and most of the LTDB-related issues have been addressed in early 2023. More than 99 % of SCs are working in good condition and there are no clusters of malfunctioning SCs in May 2023.

9 Summary

The ATLAS LAr Digital Trigger system has been introduced as the Phase-I upgrade. Up to ten times higher granularity trigger readout units (Super Cells) are introduced to use EM

shower shape to suppress multi-jet backgrounds for EM triggers. This system is built for high-speed and high-density digital processing. More than 8,200 optical links with 116 FPGAs in total are used. Momentum and timing calibration has been established and 99 % of super cells are functional. In particular, the EMB trigger performance is close to what was expected in the technical design report. Since May 2023, the digital trigger system has taken over from the analog system to provide inputs to the EM trigger. LAr calorimeter's main readout is also performing as well as it did in Run-2.

10 Acknowledgments

First, I'd like to appreciate the organizers for organizing such a conference. Then I'd like to thank all of the LAr calorimeter group members to give me a chance to talk and support me for this presentation. I'd like to continue our commitment to the future operation and success of the LAr calorimeter.

References

[1] ATLAS Collaboration (2017) ATLAS Liquid Argon Calorimeter Phase-II Upgrade:Technical Design Report. CERN-LHCC-2017-018, ATLAS-TDR-027 https://cds.cern.ch/record/2285582

[2] ATLAS Collaboration (2023) Beam splash event March 28, 2023. [online] https://atlaspo.cern.ch/public/event_display/

[3] ATLAS Collaboration (2023) LAr Cell Coverage. [online] https://twiki.cern.ch/twiki/bin/view/AtlasPublic/LArCaloPublicBeamSplashMay2023

[4] ATLAS Collaboration (2022) Expected performance of the ATLAS Level-1 calorimeter trigger in Run 3. [online] https://twiki.cern.ch/twiki/bin/view/AtlasPublic/L1CaloTriggerPublicResults

[5] ATLAS Collaboration (2013) ATLAS Liquid Argon Calorimeter Phase-I Upgrade:Technical Design Report. CERN-LHCC-2013-017, ATLAS-TDR-022 https://cds.cern.ch/record/1602230

[6] Aad G., et al. (2022) The Phase-I Trigger Readout Electronics Upgrade of the ATLAS Liquid Argon Calorimeters. JINST **17** P05024 arXiv:2202.07384

[7] ATLAS Collaboration (2023) LHC Stable Beam Collisions 2022 LAr Digital Trigger Performance Plots. [online] https://twiki.cern.ch/twiki/bin/view/AtlasPublic/LArCaloPublicStableBeam2022DT

[8] ATLAS Collaboration (1996) ATLAS Liquid Argon Calorimeter : Technical Design Report. https://cds.cern.ch/record/331061

[9] ATLAS Collaboration (2022) ATLAS Level-1 calorimeter trigger Run3 comparison. Phase 1 versus Legacy system. [online] https://twiki.cern.ch/twiki/bin/view/AtlasPublic/L1CaloTriggerPublicResults

[10] ATLAS Collaboration (2008) The ATLAS Experiment at the CERN Large Hadron Collider. JINST **3** S08003.